



Published in final edited form as:

Sci Transl Med. 2015 November 18; 7(314): 314ra187. doi:10.1126/scitranslmed.aab4014.

Bioengineered vocal fold mucosa for voice restoration*

Changying Ling¹, Qiyao Li², Matthew E. Brown³, Yo Kishimoto^{1,†}, Yutaka Toya^{1,‡}, Erin E. Devine¹, Kyeong-Ok Choi⁴, Kohei Nishimoto¹, Ian G. Norman³, Tenzin Tsegayal¹, Jack J. Jiang¹, William J. Burlingham³, Sundaram Gunasekaran⁴, Lloyd M. Smith², Brian L. Frey², and Nathan V. Welham^{1,§}

¹Division of Otolaryngology, Department of Surgery, University of Wisconsin School of Medicine and Public Health, Madison, WI, USA

²Department of Chemistry, University of Wisconsin-Madison, Madison, WI, USA

³Division of Transplantation, Department of Surgery, University of Wisconsin School of Medicine and Public Health, Madison, WI, USA

⁴Department of Biological Systems Engineering, University of Wisconsin-Madison, Madison, WI, USA

Abstract

Patients with voice impairment caused by advanced vocal fold (VF) fibrosis or tissue loss have few treatment options. A transplantable, bioengineered VF mucosa would address the individual and societal costs of voice-related communication loss. Such a tissue must be biomechanically capable of aerodynamic-to-acoustic energy transfer and high-frequency vibration, and physiologically capable of maintaining a barrier against the airway lumen. Here, we isolated primary human VF fibroblasts and epithelial cells and cocultured them under organotypic conditions. The resulting engineered mucosae showed morphologic features of native tissue, proteome-level evidence of mucosal morphogenesis and emerging extracellular matrix

*This manuscript has been accepted for publication in Science Translational Medicine. This version has not undergone final editing. Please refer to the complete version of record at www.sciencetranslationalmedicine.org. The manuscript may not be reproduced or used in any manner that does not fall within the fair use provisions of the Copyright Act without the prior, written permission of AAAS.

§To whom correspondence should be addressed: welham@surgery.wisc.edu.

†Currently affiliated with: Department of Otolaryngology, Kyoto University, Kyoto, Japan.

‡Currently affiliated with: Department of Otolaryngology, Kumamoto University, Kumamoto, Japan.

Author contributions: C.L. designed experiments, performed all *in vitro* experiments, analyzed data, and helped write the manuscript. Q.L. designed experiments, performed proteomic assays, analyzed data, and helped write the manuscript. M.E.B. designed experiments, performed *in vivo* transplantation experiments, and analyzed data. Y.K. and Y.T. performed all laryngeal surgical procedures and *ex vivo* experiments. E.E.D. analyzed *ex vivo* experimental data. K.-O.C. performed rheologic assays and analyzed data. K.N. performed dissections and analyzed data. I.G.N. helped perform *in vivo* transplantation experiments. T.T. helped perform *in vitro* experiments and analyzed data. J.J.J. provided input on the *ex vivo* experimental data analysis and reviewed the manuscript. W.J.B. provided input on the *in vivo* transplantation experiments and reviewed the manuscript. S.G. provided input on the rheologic assays and analyzed data. L.M.S. provided input on the proteomic data analysis and reviewed the manuscript. B.L.F. helped design the experiments, performed proteomic data analysis, and reviewed the manuscript. N.V.W. conceived the study, designed the experiments, performed *ex vivo* experiments, analyzed data, and helped write the manuscript.

Competing interests: The authors declare no competing financial interests. The Wisconsin Alumni Research Foundation has filed a provisional United States patent on the tissue engineering technology, with C.L. and N.V.W. as inventors.

Data and materials availability: The raw MS data files are available from the PeptideAtlas repository [<http://www.peptideatlas.org>] using the dataset identifier PASS00271.

complexity, and rudimentary barrier function *in vitro*. When grafted into canine larynges *ex vivo*, the mucosae generated vibratory behavior and acoustic output that were indistinguishable from those of native VF tissue. When grafted into humanized mice *in vivo*, the mucosae survived and were well tolerated by the human adaptive immune system. This tissue engineering approach has the potential to restore voice function in patients with otherwise untreatable VF mucosal disease.

Introduction

Voice impairment, called dysphonia, affects an estimated 20 million people in the United States, resulting in reduced quality of life (1), reduced occupational performance and attendance (2), and direct health care costs exceeding \$11 billion per year (3). Between 60 and 80% of voice complaints in the treatment-seeking population involve changes to the vocal fold (VF) mucosa (4); mucosal impairment or loss due to trauma, disease, or disease resection can cause fibrosis and deterioration of VF vibratory capacity for voice (5). Patients with substantial VF mucosal damage have limited treatment options. Medialization of the impaired VF, achieved by delivering an implant or injectate to the paraglottic space (6), can improve VF closure and therefore voice, but does not address fibrotic changes to the extracellular matrix (ECM). Superficial injection of a regenerative biomaterial can improve VF viscoelasticity and vibratory function (7); however, most biomaterials are not engineered for the VF biomechanical environment, have limited residence time, and cannot replace large tissue deficits. Creation of a bioengineered VF mucosa could bypass these challenges by providing tissue for transplantation that is biomechanically appropriate as a sound source for voice production, and physiologically capable of maintaining a barrier against the airway lumen.

Tissue engineering of partial and complete VF mucosae has been attempted using decellularized ECM (8), collagen (9, 10), and fibrin (11, 12) scaffolds, often seeded with pluripotent stem cell derivatives (10), multipotent stem cells (11, 12), or somatic cells (8, 9). These organotypic cultures have yielded engineered mucosae with desirable histologic features; however, to date, there is no benchmark system based on human-sourced VF primary cells against which stem cell-based approaches can be evaluated. Furthermore, organotypic cultures have not been directly compared to native human VF mucosa to show equivalent morphology and protein distribution, and most importantly, limited progress has been made toward restoration of physiologic function (12). Advances in the field of VF tissue engineering have been hampered by limited access to disease-free primary human VF mucosal cells (13) and inadequate attention to the protein- and anatomic substructure-level complexity that characterizes mucosal morphogenesis.

We hypothesized that primary human-sourced VF mucosal cells, exposed to unique mechanical forces during human voice production (14), could be an appropriate cell source for the development of a bioengineered VF mucosa capable of recapitulating native function. We therefore isolated and purified primary vocal fold fibroblasts (VFF) and epithelial cells (VFE) from human donors and cultured these cells under 3D organotypic conditions, based on techniques commonly used in skin and other mucosal systems (15, 16). The resulting engineered mucosae showed morphologic resemblance to native human VF

mucosa, proteome-level evidence of organogenesis/morphogenesis with emerging ECM complexity, and rudimentary epithelial barrier function *in vitro*. Using a large animal (canine) construct *ex vivo*, we observed aerodynamic-to-acoustic energy transfer, periodic VF vibration with physiologic mucosal wave travel, and acoustic output that were each indistinguishable from those generated by native tissue. We further implanted engineered VF mucosal auto- and allografts *in vivo* in a humanized mouse and documented robust graft survival with tolerance by the human adaptive immune system.

Results

Isolation and characterization of primary cells from human VF mucosa

Primary VF mucosal cell culture is rarely feasible with disease-free tissue from human donors, as elective biopsy carries an unacceptable risk of scar formation and dysphonia. For this reason, and because of associated technical challenges, there are no published reports, to our knowledge, of concurrent isolation and primary culture of VFF and VFE from a human donor. We obtained human tissue from a cadaver at autopsy (< 6 h postmortem) and from patients undergoing total laryngectomy for indications that did not include VF pathology (table S1), and initially conducted explant culture in fibroblast- or epithelial cell-oriented medium. Fibroblast-oriented culture resulted in steady VFF proliferation and deletion of non-target cells, yielding a morphologically pure VFF population within 21 d (fig. S1A). Conversely, epithelial cell-oriented culture resulted in limited VFE proliferation alongside growth of non-epithelial cells, including those with fibroblastic morphology. We observed tangling of various cell subpopulations (fig. S1B) and heterogeneous cell sphere formation leading to problems with reattachment during culture passage.

Given these findings, we developed an approach to better isolate and purify VFF and VFE, which briefly involved microdissection; enzymatic digestion to release cells from the ECM; and separation of cells into VFF and VFE subpopulations based on their adhesion to ECM-coated surfaces (Fig. 1A). The primary cells were then cultured separately under respective fibroblast- or epithelial cell-oriented conditions. VFF formed large colonies 10–15 d post-seeding; most cells contained classic-appearing spindle/starlike somata and elongated processes (Fig. 1B). VFE formed colonies 20–25 d post-seeding; most cells contained large nuclei, cuboidal somata, and short processes.

Fibroblasts and epithelial cells exhibit distinct cellular markers *in vivo* but share expression of most markers, at different abundances, *in vitro* (17, 18). We used a 6-marker flow cytometry panel to characterize the relative expression of classic fibroblast (prolyl-4-hydroxylase β [P4HB]; CD90, also known as Thy-1) and epithelial (pan-keratin [KRT]; KRT14; KRT19; CD227, also known as epithelial membrane antigen or mucin 1) proteins in our adhesion-separated VFF and VFE (Fig. 1C). Relative expression levels (based on low/high gating) were consistent with cell phenotype; however, single-marker analysis was ineffective at completely separating the two subpopulations. Subsequent double staining resulted in successful separation into CD90^{hi}CD227^{lo} (VFF) and CD90^{lo}CD227^{hi} (VFE) subpopulations (Fig. 1D), confirming the effectiveness of our isolation and purification workflow.

VFF maintained a consistent proliferation rate (30–40 h population doubling time) over 6 passages (Fig. 1E). VFE proliferated more slowly overall, initially maintaining a 55–65 h population doubling time that progressively increased across passages 4–6. We therefore used passage 3 cells for subsequent experiments.

Assembly of engineered VF mucosa

We pursued 3D organotypic culture with purified human primary cells in polymerized type I collagen, a core ECM constituent of native human VF mucosa (19). Initial trials using 2×10^5 VFF/mL, without VFE, resulted in an intra-scaffold cell density comparable to the non-vascular region of the native lamina propria (medium cell density, fig. S2A) and ~50% of the cell density of the entire vascularized native lamina propria (fig. S2B). We observed moderate scaffold contraction over the first 96 h of culture (fig. S2C), which corresponded to expression of a subset of matrix metalloproteinase (MMP) and tissue inhibitor of metalloproteinase (TIMP) enzymes/inhibitors (fig. S2D), as well as the contractile protein α -actin 2 (ACTA2; also known as α -smooth muscle actin) (fig. S2E). We maintained the 2×10^5 VFF/mL seeding density in subsequent experiments, followed by VFE seeding at 24 h, media-immersed VFF-VFE coculture for 48 h, and coculture with VFE at the air-liquid interface for a further 8–28 d (fig. S3).

The engineered VF mucosa began to resemble native mucosa after 10–14 d, exhibiting a ~50 μ m-thick stratified squamous epithelium and sparsely cell populated lamina propria (Fig. 2A). Basal VFE processes extended into the underlying lamina propria, consistent with epithelial anchoring. The lamina propria contained glycosaminoglycans (GAGs), including the biomechanically important GAG hyaluronic acid (20) (fig. S4A); however, its ECM appeared immature overall, populated by sparsely distributed fibers that did not resemble the sophisticated ECM of native mucosa (fig. S4B). P4HB⁺ VFF were identified throughout the lamina propria, and P4HB⁺ VFE were preferentially localized to the basal epithelium near the basement membrane, as seen in native mucosa (Fig. 2B). Basal VFE also expressed the basement membrane marker type IV collagen (COL4), which formed a barrier-like structure in the subepithelium. Unlike native mucosa, however, a comparable COL4⁺ structure was also observed at the luminal epithelial surface. The majority of VFE were E-cadherin (CDH1)⁺, suggesting emergence of intercellular junctional complexes that approximated those seen in native VF mucosa.

To further characterize the biological complexity of the engineered VF mucosa, we conducted discovery proteomic analysis using liquid chromatography-tandem mass spectrometry (LC-MS/MS). Using a 1% false discovery rate (FDR), we identified 762 unique proteins in the engineered mucosa, compared with 908 in the native mucosa and 32 in the scaffold (Fig. 2C; table S2). Gene ontology enrichment analysis of the engineered VF mucosa proteome, compared to the full human protein database (Uniprot), revealed a wide complement of protein sets (ontology terms) associated with various metabolic, catalytic, transport, binding, and signaling functions; spanning an array of subcellular and extracellular locations (Fig. 2D; table S3). We identified organogenesis/morphogenesis-specific ontology term enrichment, consistent with successful organotypic culture; as well as ECM terms indicative of protein complexes and anatomic substructures that are

characteristic of native VF mucosa, such as the basal lamina, anchoring collagen, and fibrillar collagen (fig. S5). Normalized spectral abundance factor (NSAF)-based quantitative analysis (21) showed that ECM protein abundances in the engineered mucosa were more similar to the native mucosa than the scaffold (z score shift = 0.46 ± 1.35 versus 3.65 ± 1.68 [means \pm SD, $n = 76$ proteins]; $P < 0.0001$, Student's t test) (Fig. 2E; table S4), confirming that the engineered mucosa ECM is mostly attributable to new protein synthesis by VFF and VFE.

We identified ECM proteins and glycoconjugates that are considered critical to the biomechanical function of native VF mucosa (22, 23), including multiple collagen isoforms; the elastin conduit fibrillin 1 and elastin microfibril interface-located protein (EMILIN) 1; the small leucine-rich repeat proteoglycans decorin, lumican and biglycan; and the glycoproteins fibronectin, fibulin 1 and tenascin X. These observations suggest that while the engineered lamina propria appeared immature on histologic analysis, its developing ECM has the potential to support vibratory function. This conclusion was further supported by rheologic experiments showing similar viscoelastic profiles for engineered and native mucosae (Fig. 2F).

Quantitative proteomic analysis of engineered VF mucosa compared to its isolated subcomponents

We sought to identify protein complexes and functionality that were unique to the engineered VF mucosa, compared to its isolated subcomponents: VFF in a type I collagen scaffold or VFE on a type I collagen scaffold. Proteome coverage was comparable, with 528 proteins common to all three cultures and 59 proteins unique to the engineered mucosa (Fig. 3A; table S2). Comparison of the abundance (NSAF values) of each protein showed that the majority of differentially abundant proteins were overrepresented in the engineered mucosa compared to the other conditions (Fig. 3B), suggesting that certain proteins are upregulated owing to VFF-VFE synergy in organotypic culture. The engineered mucosa was more similar to VFE on scaffold than VFF in scaffold (69 versus 139 differentially abundant proteins, respectively) (fig. S6; table S5), consistent with VFE being its predominant cell type.

Next, we performed enrichment analysis of the protein set that was either exclusively identified or overrepresented in engineered VF mucosa compared to both VFF in scaffold and VFE on scaffold. The most highly represented biological process terms indicated that the engineered mucosa was uniquely engaged in macromolecule catabolism, protein localization, and cellular component organization or biogenesis (Fig. 3C). Additional relevant terms included cell-substrate junction assembly, epidermis development, adherens junction organization and cell junction assembly (table S6). Enrichment of these terms was driven by a common protein set consisting of the basal lamina constituent laminin α -5 (LAMA5), the basal epithelial cell marker KRT5, the desmosome constituents junction plakoglobin (JUP, also known as γ -catenin) and periplakin (PPL), and type V collagen α -1 (COL5A1).

Emergence of immature barrier function in engineered VF mucosa

Our histologic and proteomic data suggested the emergence of basement membrane structures and epithelial junctional complexes during organotypic culture. We therefore performed immunovalidation of LAMA5, KRT5, and JUP expression in engineered VF mucosa, and compared their distribution to native VF mucosa. Each protein was expressed in the engineered epithelium but lacked the region-specific localization of native epithelium (Fig. 3D). LAMA5 was expressed by basal and suprabasal VFE and showed intracellular colocalization with its functional partner COL4, but these proteins did not form mature basal laminae. KRT5⁺ VFE were scattered throughout the engineered epithelium but were not preferentially localized to the basal region. JUP was expressed by the majority of VFE and colocalized with its binding partner CDH1, but these proteins did not exhibit the intercellular distribution pattern of mature junctional complexes within native epithelium.

To further evaluate physiologic barrier function in the engineered mucosa, we conducted transmucosal electrical resistance experiments. This required decreasing fibroblast seeding density by ~3.5-fold (to 5.6×10^4 VFF/mL) to reduce scaffold contraction and eliminate detachment from the insert wall. Under comparable culture conditions, the engineered mucosa had significantly greater resistance than scaffold only and VFF in scaffold, but not VFE on scaffold (Fig. 3E). These data corroborate our immunohistochemical data and confirm that, although emerging basement membrane and epithelial junctional complexes were present in the engineered mucosa, physiologic barrier function remained immature.

Ex vivo physiologic function of engineered VF mucosa

We scaled-up our engineering approach to create human-sized VF mucosae and evaluated their physiologic performance in a large animal (canine) excised larynx. This *ex vivo* approach holds methodological advantages over *in vivo* techniques, owing to greater control of anatomic, postural, and aerodynamic input parameters; direct visual exposure of the VFs during vibration; and more precise measurement. We used canine larynges based on their anatomic similarity to humans and precedence in excised larynx studies (24). Sequential datasets were collected from each larynx: (i) with bilateral native VFs intact, (ii) following unilateral mucosal resection to impair physiologic function, and (iii) following unilateral placement of engineered mucosa in an attempt to restore function (fig. S7A).

We collected aerodynamic, high-speed digital imaging (HSDI) and acoustic data (fig. S7B). Following arytenoid adduction, we delivered humidified air at gradually increasing subglottal pressures (P_s) to initiate flow (U)-induced VF vibration. The minimum P_s required to initiate vibration (phonation threshold pressure, P_{th}) was ~1 kPa in the native condition but increased to >5 kPa following resection (Fig. 4A). Placement of engineered mucosa restored vibration with comparable P_{th} to the native condition. Native and engineered mucosae exhibited similar within-larynx glottal resistance (R_g), aerodynamic input power (\wp_{aero}), radiated acoustic power (\wp_{ac}), and glottal efficiency (E_g). \wp_{aero} to \wp_{ac} loss resulted in E_g values of 0.01 to 0.0001% across all runs, consistent with previously reported data from canine excised larynx experiments (24).

HSDI analysis showed restoration of typical vibratory physiology following engineered VF mucosa replacement. Glottal area waveforms and displacement values were similar to those generated by native mucosa, particularly for within-larynx comparisons (Fig. 4B). Engineered mucosa vibrated with a vertical phase difference between upper and lower margins, intact mucosal wave, and lateral (left-right) phase symmetry with the contralateral VF (Fig. 4C; movie S1). Using HSDI-extracted kymograms, we fitted sinusoidal curves to the upper and lower margins of each VF and observed comparable phase differences for all comparisons (Fig. 4D).

Acoustic analysis confirmed these vibratory physiology findings, showing restoration of signal periodicity, harmonic structure, and closed phase trajectories following placement of engineered mucosa (Fig. 4E; movie S2). Using narrow-band spectrography-based qualitative signal typing (25), acoustic signals generated by native and engineered mucosae were uniformly categorized as type 1 (near-periodic), whereas signals associated with mucosal resection were uniformly categorized as type 4 (stochastic) (Fig. 4F). In total, the aerodynamic, vibratory, and acoustic performance of the engineered mucosa was functionally equivalent to that of native tissue.

Using the same *ex vivo* setup (fig. S7), we next compared the physiologic function of engineered VF mucosa to human oral mucosa, a traditional free graft material used for reconstructing large VF mucosal deficits (26, 27). Oral mucosa vibrated with elevated P_{th} (Fig. 5A), as well as reduced glottal area magnitude and mucosal wave excursion (Fig. 5, B and C), suggesting reduced tissue compliance and a poor viscosity match to native VF mucosa (14, 28). Vibratory phase differences were comparable across the oral and engineered VF mucosa conditions (Fig. 5D) and oral mucosa generated type 1 acoustic signals with harmonic structure in most experimental runs (Fig. 5, E and F). These data indicate that although both materials are capable of vibration and acoustic output, engineered VF mucosa has superior tissue compliance to oral mucosa—the standard-of-care in current surgical practice.

Immunogenicity of engineered VF mucosa

To evaluate its potential for therapeutic implementation, we tested the immunogenicity of engineered VF mucosa and its constituent cells using flow cytometry and an *in vivo* transplantation assay. Previous work has shown that primary VFF express a cell-surface phenotype that is comparable to immunoprivileged multipotent stem cells (29), however no such data have been reported for VFE. VFF and VFE uniformly expressed the pan-major histocompatibility complex (MHC) class I marker human leukocyte antigen (HLA)-ABC (common to all nucleated cells), but were negative for the pan-MHC class II marker HLA-DR (associated with professional antigen-presenting cells), as well as the T cell costimulatory molecules CD80 and CD86 (Fig. 6A). Further, 45–75% of VFF and VFE expressed the T cell inhibiting and tolerance-promoting molecules programmed death-ligand (PD-L) 1 and PD-L2 (also known as CD274 and CD273, respectively). These findings suggest that naïve VFF and VFE have limited antigen-presentation capacity and may promote immunotolerance.

We next evaluated *in vivo* survival and tolerance of engineered VF mucosa following subrenal capsule auto- and allograft transplantation in the humanized NOD-*scid IL2r γ ^{null}* (NSG) mouse (30). The NSG model supports engraftment of human peripheral blood lymphocytes (hPBL) and establishment of a functional human adaptive immune system, allowing evaluation of graft immunogenicity prior to terminal xenogeneic graft-versus-host disease (GVHD). We implanted engineered VF mucosal grafts from unrelated human donors under the bilateral renal capsules of irradiated NSG mice, followed by intravenous delivery of 13×10^6 hPBL that were autologous to one of the two grafts (fig. S8). Mice exhibited a significant decrease in body mass (Fig. 6B) and progressive onset of GVHD. Flow cytometry confirmed engraftment and proliferation of hCD45⁺mCD45⁻ human lymphocytes in mouse peripheral blood (Fig. 6C).

Fifteen to 21 days after hPBL engraftment, there was a predominant infiltration of hCD4⁺ T helper cells and minimal infiltration of hCD8⁺ cytotoxic T cells, with no difference between the auto- and allografts (Fig. 6D). Follow-up analysis of forkhead box P3 (hFOXP3) coexpression by the infiltrating hCD4⁺ cells revealed a significantly higher subpopulation of hCD4⁺hFOXP3⁺ regulatory T cells in the engineered auto- and allografts compared to the mouse eyelid, a GVHD-affected positive control tissue (Fig. 6E). This finding corresponded to preservation of tissue morphology in the engineered auto- and allografts, which contrasted with extensive cellular infiltration and destruction of naïve tissue morphology in the mouse eyelid (Fig. 6F).

The identification of a robust subpopulation of regulatory T cells in the auto- and allografts, combined with the absence of tissue destruction in both conditions, suggests that engineered VF mucosa holds low immunogenicity and is well tolerated by the human adaptive immune system *in vivo*. Additional long-term experiments in NSG mice without hPBL challenge confirmed that the grafts survived and remained populated by human cells for 70 to 98 d (Fig. 6B; fig. S9A). The acellular scaffold exhibited comparable long-term survival (fig. S9B). When implanted in hPBL-induced humanized NSG mice, the scaffold exhibited no hCD45⁺ lymphocyte infiltration (fig. S9C) despite GVHD in the host, indicating absence of recognition by the human adaptive immune system. This observation is consistent with previous reports of minimal host response to xenogeneic collagen in human clinical applications.

Discussion

We have met a series of milestones toward the development of a bioengineered VF mucosa suitable for therapeutic transplantation. In this study, we demonstrate concurrent isolation and purification of primary VFF and VFE from individual human donors; 3D organotypic culture resulting in recapitulation of key morphologic features and emerging barrier function; confirmation of size scalability by adapting for canine larynges; restoration of native-appearing physiologic vibratory function and acoustic output after VF resection; and tolerance by the human adaptive immune system. The biomechanical performance and low immunogenicity of this engineered mucosa indicate that our approach could restore voice function in patients with otherwise untreatable VF mucosal impairment.

We used primary human VFF and VFE assuming that these cells are ideally suited for VF organotypic culture owing to their exposure to phonation-associated mechanical forces *in vivo* (14). This approach was successful, and under permissive conditions the cells engaged in mucosal morphogenesis, contributing to assembly of a functional 3D tissue. Given that primary VF mucosal cells are not available for large-scale therapeutics, use of alternative populations, such as pluripotent stem cell derivatives (10), bone marrow- (31) or adipose-derived multipotent stem cells (11, 12), or non-VF somatic cells (32), is an attractive future direction. Such cells might be differentiated toward a VF mucosal cell phenotype, and primed for organotypic culture and transplantation, by exposure to tensile and vibratory forces in a laryngeal bioreactor (33).

VF vibration and mucosal wave travel are dependent on tissue viscoelasticity (14), which in turn is a function of VFF-secreted ECM composition (22, 23). We seeded cells in a simple type I collagen-based scaffold, selected for its cytocompatibility, abundance in native human VF mucosa, and use in previous organotypic cultures and engineered tissues (15, 16, 19). The scaffold was augmented by endogenous ECM production by the seeded cells, and the engineered mucosa was further strengthened by VFF-driven contraction to the point that it was able to withstand physiologically relevant driving pressures (~1–3 kPa) and frequencies (~100–300 Hz) for 10–15 min *ex vivo*. Still, although physiologic function was comparable, the engineered mucosa did not show lamina propria fiber complexity equivalent to that of native mucosa. This is not surprising considering that, during human development, differentiation of the lamina propria into a complex structure with depth-dependent fibrous protein distribution begins at postnatal age 2 mo and is not complete until at least 13 y (34). Extended culture time, phonation-relevant dosing with mechanical forces (33), and/or the use of more architecturally relevant scaffold materials, such as decellularized VF mucosa (35), might provide the microenvironmental cues needed to yield even greater maturation *in vitro*.

The engineered VF mucosa exhibited low immunogenicity when presented to the human adaptive immune system *in vivo* in mice, suggesting that our primary cell-based approach itself has clinical potential for allotransplantation. Development of this approach beyond proof-of-principle requires orthotopic transplantation experiments, with evaluation of long-term tolerance and physiologic outcomes. Such experiments could be pursued using translationally relevant canine or porcine models and may also help determine how *in vivo* incorporation of host cells and ongoing ECM remodeling further the regeneration process. Free mucosal graft is a technically straightforward procedure in patient laryngeal reconstruction and, given its limited vascular demand, has high viability post-grafting (27). Key considerations in determining *in vivo* outcomes, therefore, may be the relative immunoprivilege of the (primary or non-primary) cells used for organotypic culture, as well as the impact of the host response and local biomechanical environment on long-term graft remodeling.

In summary, this report provides a framework for the efficient generation of physiologically relevant and clinically useful bioengineered VF mucosae. Beyond its direct potential for therapeutic use, this approach has application to the development of advanced *in vitro* systems for VF mucosal disease modeling and preclinical testing of therapeutic agents.

Materials and Methods

Study Design

Our objective was to engineer human VF mucosa with functional performance comparable to that of native tissue. Cell characterization experiments were performed using primary cells isolated from a cadaver and surgical patients. The engineering strategy involved organotypic coculture of primary VFF and VFE; initial characterization was performed using histology and immunohistochemistry, proteomics, rheology, protein array, and electrical resistance. *Ex vivo* physiology experiments were conducted using canine larynges and sequential data collection at baseline, following unilateral VF mucosa resection, and following engineered mucosae placement; the contralateral VF served as a within-larynx native tissue control. *In vivo* immunogenicity experiments were conducted using a humanized mouse system and within-animal comparisons of auto- and allograft outcomes. Animals were not randomized. All human and animal procedures were performed with institutional approvals and, in the case of human participants, with informed consent.

All analyses were performed on blinded samples. For functional assays, pilot data were collected with $n = 3$ replicates followed by calculation of the necessary sample size to detect a >1 SD shift with 80% power. The 14 d endpoint for organotypic culture was determined by a pilot experiment showing no morphological differences at 14 and 28 d. Endpoints for the *in vivo* experiment were determined by onset of xenogeneic GVHD (in mice with hPBL) or monitoring for at least $3\times$ the longest survival time in the hPBL group (in mice with no hPBL).

Cell isolation and culture

Human VF mucosae ($n = 10$) were obtained from a single cadaver at autopsy (< 6 h postmortem) and 4 patients undergoing total laryngectomy with no evidence of VF pathology on otolaryngologic work-up (table S1). Procurement was performed with approval of the University of Wisconsin-Madison Health Sciences Institutional Review Board. Each mucosa was microdissected from its underlying thyroarytenoid muscle and processed as described in Supplementary methods.

Organotypic culture

We engineered 167 VF mucosae using 3D organotypic culture. Purified rat tail type I collagen was seeded with VFF and polymerized. After 24 h of VFF culture, VFE were seeded on the scaffold surface. After 48 h of VFF-VFE coculture, medium was aspirated from the apical chamber. We continued coculture with VFE at the air-liquid interface for a further 8–28 d. Additional details are provided in Supplementary methods.

As initial histological assessment showed no difference in engineered VF mucosa morphology at 14 and 28 d, we performed all subsequent downstream assays on samples harvested at 14 d. Experimental comparisons involving the scaffold only, VFF in scaffold and VFE on scaffold involved identical culture conditions for the entire 14 d period.

Ex vivo physiology experiments

Ex vivo physiologic data from canine larynges with bilateral native VFs intact, following unilateral VF mucosa resection, and following unilateral placement of either engineered VF mucosa or oral mucosa were collected as described in Supplementary methods.

Humanized mouse experiments

NOD-*scid* *IL2r γ ^{null}* (NSG) mice aged 7–8 wk ($n = 22$; Jackson Laboratory) and hPBL were used for all *in vivo* experiments, as described in Supplementary methods.

Proteomic analyses

Protein extraction, tryptic digestion, MS and NSAF-based quantification were performed as described in Supplementary methods.

Statistical analyses

NSAF-based quantitative proteomic data were analyzed using a Student's *t* test with Benjamini-Hochberg adjustment. Gene ontology term enrichment analysis was performed using the BiNGO (hypergeometric model with Benjamini-Hochberg adjustment) and REVIGO algorithms. Enrichment schematics were generated using Cytoscape 2.8.2 (Cytoscape Consortium). Other statistical testing was performed using SAS 9.2 (SAS Institute). Flow cytometry, rheology (slopes of each fitted curve), cell density, transmucosal resistance, P_{th} , and body mass (overall percentage change) data were analyzed using a Student's *t* test in cases of two experimental groups, or one-way ANOVA in cases of >2 experimental groups. Glottal area and vibratory phase data were analyzed using two-way ANOVA, with VF mucosa condition and P_{th} as fixed effects. Cell proliferation data were also analyzed using two-way ANOVA, with cell type and culture passage as fixed effects. Data were evaluated for normality and equality of variance using visual inspection of raw data plots and Levene's test; data were rank-transformed where needed to meet the assumptions of the Student's *t* test and ANOVA. In all ANOVA models, if the *F* test revealed a significant difference, pairwise comparisons were performed using Fisher's protected least significant difference method. Acoustic signal typing data were analyzed using a χ^2 test. A pre-adjustment type I error rate of 0.01 was used; quantitative proteomic data were subject to an additional fold change cutoff of 4. All *P* values were two-sided.

Supplementary Material

Refer to Web version on PubMed Central for supplementary material.

Acknowledgments

We thank E.G. Brooks, J.L. Corbit, T. Enters, S.H. Dailey, G.K. Hartig and T.M. McCulloch for procuring tissue; B.D. Clarkson, S.J. Ollar and Z. Fabry for assistance with transmucosal electrical resistance assays; M. Scalf for assistance with LC-MS/MS; S. Kinoshita and D.A. Roenneburg for tissue processing and histology; C.J. Brown for video editing; G.E. Levenson and S. Saha for assistance with statistical analyses.

Funding: This work was supported by grants R01 DC004428 and R01 DC010777 from the NIDCD and grant R01 AI066219 from the NIAID. M.E.B. was supported by training grant T32 GM081061 from the NIGMS; E.E.D. was supported by training grant T32 DC009401 from the NIDCD. Flow cytometry was performed in the Flow

Cytometry Laboratory of the University of Wisconsin Carbone Cancer Center, which is supported by grant P30 CA014520 from the NCI.

REFERENCES AND NOTES

1. Cohen SM, Dupont WD, Courey MS. Quality-of-life impact of non-neoplastic voice disorders: a meta-analysis. *Ann Otol Rhinol Laryngol.* 2006; 115:128–134. [PubMed: 16514796]
2. Cohen SM, Kim J, Roy N, Asche C, Courey MS. The impact of laryngeal disorders on work-related dysfunction. *Laryngoscope.* 2012; 122:1589–1594. [PubMed: 22549455]
3. Cohen SM, Kim J, Roy N, Asche C, Courey MS. Direct health care costs of laryngeal diseases and disorders. *Laryngoscope.* 2012; 122:1582–1588. [PubMed: 22544473]
4. Coyle SM, Weinrich BD, Stemple JC. Shifts in relative prevalence of laryngeal pathology in a treatment-seeking population. *J Voice.* 2001; 15:424–440. [PubMed: 11575638]
5. Friedrich G, Dikkers FG, Arens C, Remacle M, Hess MM, Giovanni A, Duflo SM, Hantzakos AG, Bachy V, Gugatschka M. Vocal fold scars: current concepts and future directions. Consensus report of the phonosurgery committee of the European laryngological society. *Eur Arch Otorhinolaryngol.* 2013; 270:2491–2507. [PubMed: 23605306]
6. Zeitels SM, Healy GB. Laryngology and phonosurgery. *N Engl J Med.* 2003; 349:882–892. [PubMed: 12944575]
7. Caton T, Thibeault SL, Klemuk S, Smith ME. Viscoelasticity of hyaluronan and nonhyaluronan based vocal fold injectables: implications for mucosal versus muscle use. *Laryngoscope.* 2007; 117:516–521. [PubMed: 17334315]
8. Xu CC, Chan RW, Tirunagari N. A biodegradable, acellular xenogeneic scaffold for regeneration of the vocal fold lamina propria. *Tissue Eng.* 2007; 13:551–566. [PubMed: 17518602]
9. Yamaguchi T, Shin T, Sugihara H. Reconstruction of the laryngeal mucosa. A three-dimensional collagen gel matrix culture. *Arch Otolaryngol Head Neck Surg.* 1996; 122:649–654. [PubMed: 8639298]
10. Leydon C, Selekman JA, Palecek S, Thibeault SL. Human embryonic stem cell-derived epithelial cells in a novel in vitro model of vocal mucosa. *Tissue Eng Part A.* 2013; 19:2233–2241. [PubMed: 23672433]
11. Long JL, Zuk P, Berke GS, Chhetri DK. Epithelial differentiation of adipose-derived stem cells for laryngeal tissue engineering. *Laryngoscope.* 2010; 120:125–131. [PubMed: 19856398]
12. Long JL, Neubauer J, Zhang Z, Zuk P, Berke GS, Chhetri DK. Functional testing of a tissue-engineered vocal fold cover replacement. *Otolaryngol Head Neck Surg.* 2010; 142:438–440. [PubMed: 20172395]
13. Chen X, Thibeault SL. Novel isolation and biochemical characterization of immortalized fibroblasts for tissue engineering vocal fold lamina propria. *Tissue Eng Part C Methods.* 2009; 15:201–212. [PubMed: 19108681]
14. Titze IR. The physics of small-amplitude oscillation of the vocal folds. *J Acoust Soc Am.* 1988; 83:1536–1552. [PubMed: 3372869]
15. Gangatirkar P, Paquet-Fifield S, Li A, Rossi R, Kaur P. Establishment of 3D organotypic cultures using human neonatal epidermal cells. *Nat Protoc.* 2007; 2:178–186. [PubMed: 17401352]
16. Dongari-Bagtzoglou A, Kashleva H. Development of a highly reproducible three-dimensional organotypic model of the oral mucosa. *Nat Protoc.* 2006; 1:2012–2018. [PubMed: 17487190]
17. von Koskull H, Virtanen I. Induction of cytokeratin expression in human mesenchymal cells. *J Cell Physiol.* 1987; 133:321–329. [PubMed: 2445764]
18. Langness U, Udenfriend S. Collagen biosynthesis in nonfibroblastic cell lines. *Proc Natl Acad Sci USA.* 1974; 71:50–51. [PubMed: 4359330]
19. Hahn MS, Kobler JB, Zeitels SM, Langer RS. Quantitative and comparative studies of the vocal fold extracellular matrix II: collagen. *Ann Otol Rhinol Laryngol.* 2006; 115:225–232. [PubMed: 16572613]
20. Chan RW, Gray SD, Titze IR. The importance of hyaluronic acid in vocal fold biomechanics. *Otolaryngol Head Neck Surg.* 2001; 124:607–614. [PubMed: 11391249]

21. Zybailov B, Mosley AL, Sardi ME, Coleman MK, Florens L, Washburn MP. Statistical analysis of membrane proteome expression changes in *Saccharomyces cerevisiae*. *J Proteome Res*. 2006; 5:2339–2347. [PubMed: 16944946]
22. Gray SD, Titze IR, Chan RW, Hammond TH. Vocal fold proteoglycans and their influence on biomechanics. *Laryngoscope*. 1999; 109:845–854. [PubMed: 10369269]
23. Gray SD, Titze IR, Alipour F, Hammond TH. Biomechanical and histologic observations of vocal fold fibrous proteins. *Ann Otol Rhinol Laryngol*. 2000; 109:77–85. [PubMed: 10651418]
24. Titze, IR. Vocal physiology: voice production mechanisms and functions. Fujimura, O., editor. Raven Press; New York: 1988. p. 227-238.
25. Sprecher A, Olszewski A, Jiang JJ, Zhang Y. Updating signal typing in voice: addition of type 4 signals. *J Acoust Soc Am*. 2010; 127:3710–3716. [PubMed: 20550269]
26. Hirano M. A technique for glottic reconstruction following vertical partial laryngectomy. *Auris Nasus Larynx*. 1978; 5:63–70. [PubMed: 751637]
27. Wang Z, Pankratov MM, Rebeiz EE, Perrault DF, Shapshay SM. Endoscopic diode laser welding of mucosal grafts on the larynx: a new technique. *Laryngoscope*. 1995; 105:49–52. [PubMed: 7837913]
28. Finkelhor BJ, Titze IR, Durham PR. The effect of viscosity changes in the vocal folds on the range of oscillation. *J Voice*. 1988; 1:320–325.
29. Hanson SE, Kim J, Quinchia Johnson BH, Bradley B, Breunig MJ, Hematti P, Thibeault SL. Characterization of mesenchymal stem cells from human vocal fold fibroblasts. *Laryngoscope*. 2010; 120:546–551. [PubMed: 20131365]
30. Shultz LD, Brehm MA, Garcia-Martinez JV, Greiner DL. Humanized mice for immune system investigation: progress, promise and challenges. *Nat Rev Immunol*. 2012; 12:786–798. [PubMed: 23059428]
31. Svensson B, Nagubothu SR, Cedervall J, Chan RW, Le Blanc K, Kimura M, Ährlund-Richter L, Tolf A, Hertegård S. Injection of human mesenchymal stem cells improves healing of vocal folds after scar excision - a xenograft analysis. *Laryngoscope*. 2011; 121:2185–2190. [PubMed: 21898432]
32. Chhetri DK, Berke GS. Injection of cultured autologous fibroblasts for human vocal fold scars. *Laryngoscope*. 2011; 121:785–792. [PubMed: 21287562]
33. Gaston J, Quinchia Rios B, Bartlett RS, Berchtold CM, Thibeault SL. The response of vocal fold fibroblasts and mesenchymal stromal cells to vibration. *PLoS One*. 2012; 7:e30965. [PubMed: 22359557]
34. Hartnick CJ, Rehbar R, Prasad V. Development and maturation of the pediatric human vocal fold lamina propria. *Laryngoscope*. 2005; 115:4–15. [PubMed: 15630357]
35. Welham NV, Chang Z, Smith LM, Frey BL. Proteomic analysis of a decellularized human vocal fold mucosa scaffold using 2D electrophoresis and high-resolution mass spectrometry. *Biomaterials*. 2013; 34:669–676. [PubMed: 23102991]
36. Yaghi A, Zaman A, Dolovich M. Primary human bronchial epithelial cells grown from explants. *J Vis Exp*. 2010:e1789.
37. Welham NV, Montequin DW, Tateya I, Tateya T, Choi SH, Bless DM. A rat excised larynx model of vocal fold scar. *J Speech Lang Hear Res*. 2009; 52:1008–1020. [PubMed: 19641079]
38. Jiang JJ, Zhang Y, Kelly MP, Bieging ET, Hoffman MR. An automatic method to quantify mucosal waves via videokymography. *Laryngoscope*. 2008; 118:1504–1510. [PubMed: 18545215]
39. Zhang Y, McGilligan C, Zhou L, Vig M, Jiang JJ. Nonlinear dynamic analysis of voices before and after surgical excision of vocal polyps. *J Acoust Soc Am*. 2004; 115:2270–2277. [PubMed: 15139638]
40. Wi niewski JR, Zougman A, Nagaraj N, Mann M. Universal sample preparation method for proteome analysis. *Nat Methods*. 2009; 6:359–362. [PubMed: 19377485]

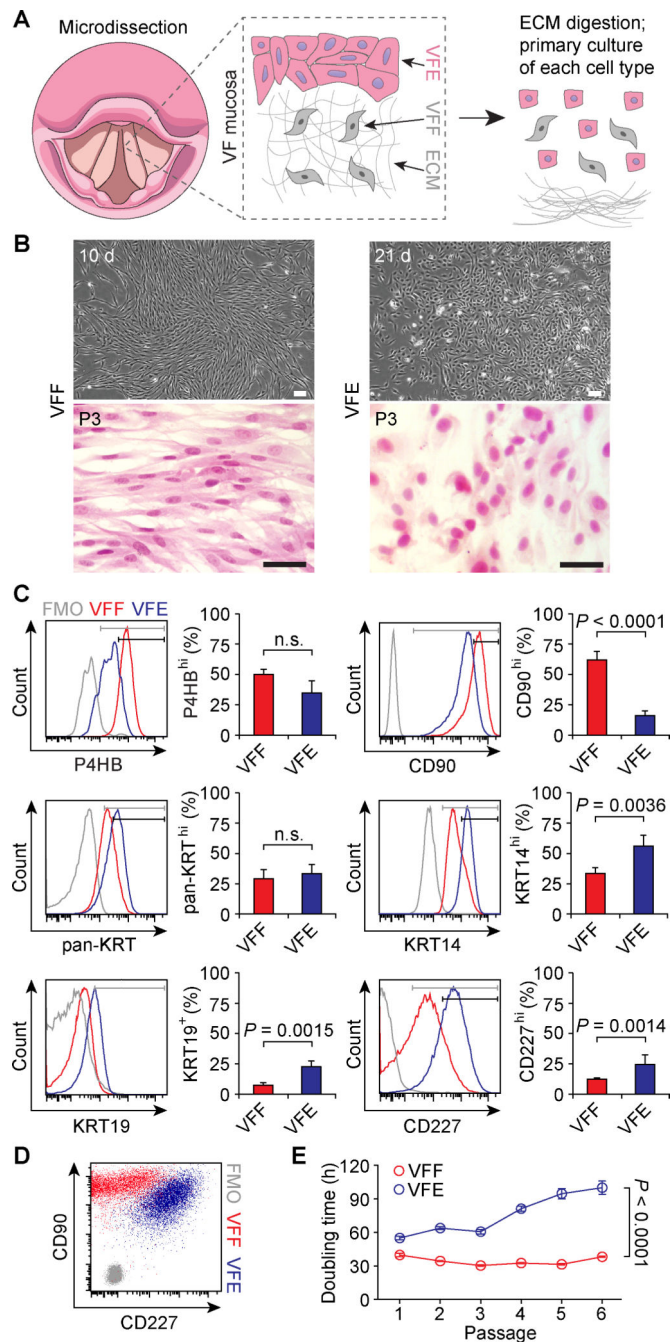


Fig. 1. Isolation, purification, and expansion of primary VFF and VFE from human VF mucosa (A) Schematic showing general procedure for fibroblast and epithelial cell isolation and purification from VF mucosa. (B) Morphology of primary VFF and VFE in monolayer culture prior to first passage (10 or 21 d post-seeding) and at passage 3 (P3, H&E staining). Scale bars, 30 μ m. (C) Expression of P4HB, CD90, pan-KRT, KRT14, KRT19, and CD227 in VFF and VFE at P3. Positive/negative gates (versus FMO control) are shown in gray; low/high gates are shown in black. Data are means \pm SEM ($n = 4-12$). P values were calculated using a Student's t test; n.s., not significant. (D) Representative CD90/CD227

double staining. (E). VFF and VFE population doubling times from P1 to P6. Data are means \pm SEM ($n = 4$). The P value was calculated using ANOVA.

Author Manuscript

Author Manuscript

Author Manuscript

Author Manuscript

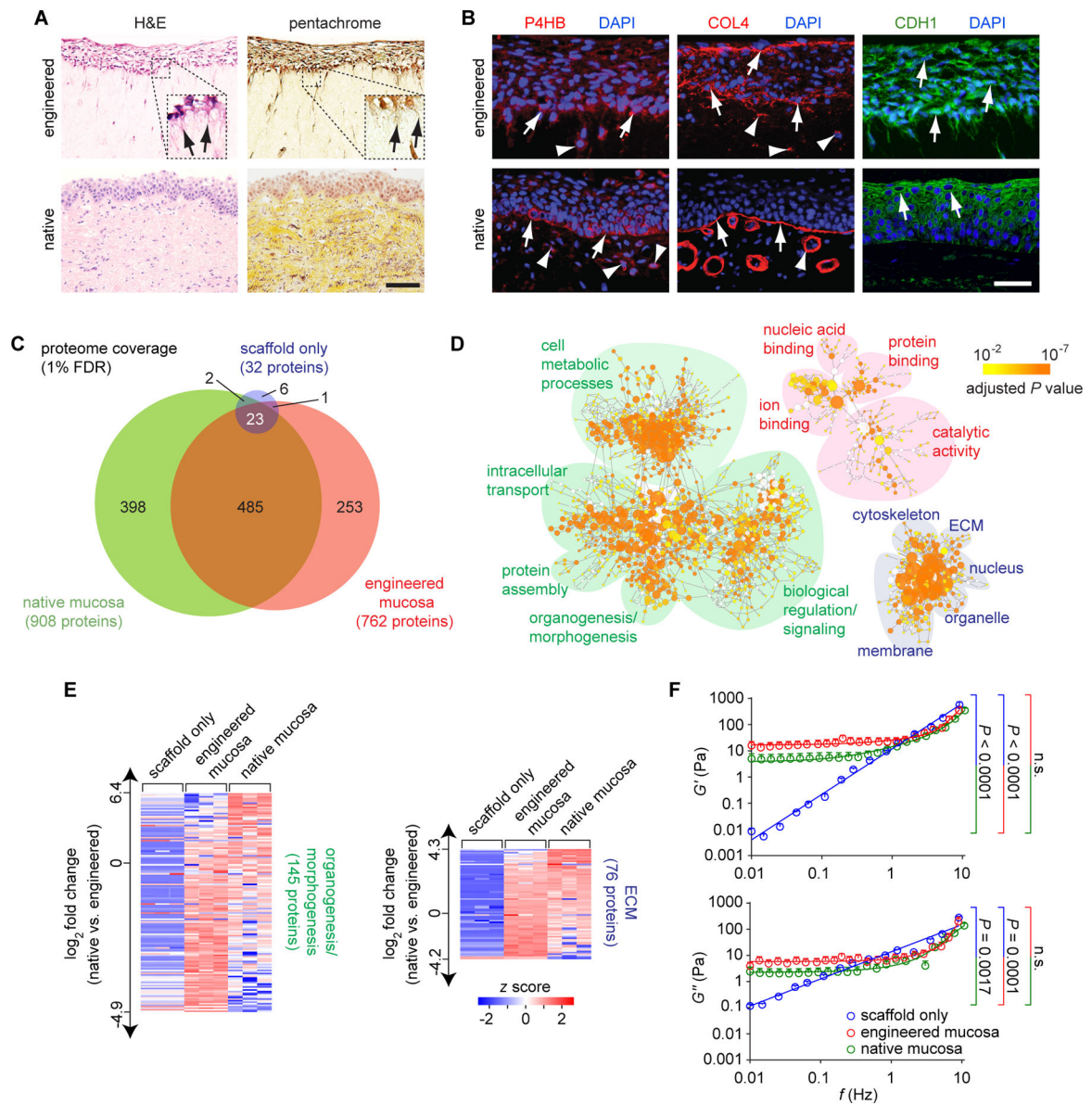


Fig. 2. Assembly of engineered human VF mucosa

(A) H&E and Movat's pentachrome (connective tissue) staining of engineered and native mucosae. Black arrows indicate basal VFE cytoplasmic projections extending into the lamina propria. Scale bar, 100 μ m; 40 μ m (insets). (B) Immunofluorescence images showing P4HB, COL4, and E-cadherin (CDH1) staining patterns. White arrows indicate P4HB⁺ VFE, COL4⁺ basement membrane and luminal epithelial structures, and CDH1⁺ VFE. White arrowheads indicate P4HB⁺ VFF and COL4⁺ VFF and vascular basement membrane structures in the lamina propria. Scale bar, 50 μ m. (C) Venn diagram summarizing proteome coverage in engineered mucosa compared to native mucosa and scaffold only. (D) Enrichment analysis of the engineered mucosa proteome. Enriched gene ontology terms are depicted as nodes connected by arrows that represent hierarchies and relationships between terms. Node size is proportional to the number of assigned proteins; node color represents

the adjusted P value (calculated using BiNGO, $n = 3$) corresponding to enrichment. Functionally related ontology terms are grouped using colored ovals (green, biological process; red, molecular function; blue, cellular component). Organogenesis/morphogenesis and ECM terms are enlarged for better visualization in fig. S6. **(E)** Heatmaps summarizing NSAF-based quantification of proteins associated with the organogenesis/morphogenesis and ECM ontology terms. A corresponding list of proteins and fold changes is presented in table S4. **(F)** Rheologic data showing elastic (G') and viscous (G'') moduli of engineered mucosa compared to native mucosa and scaffold only. Data are means \pm SEM ($n = 4-12$). P values (comparison of slopes) were calculated using ANOVA; n.s., not significant.

Author Manuscript

Author Manuscript

Author Manuscript

Author Manuscript

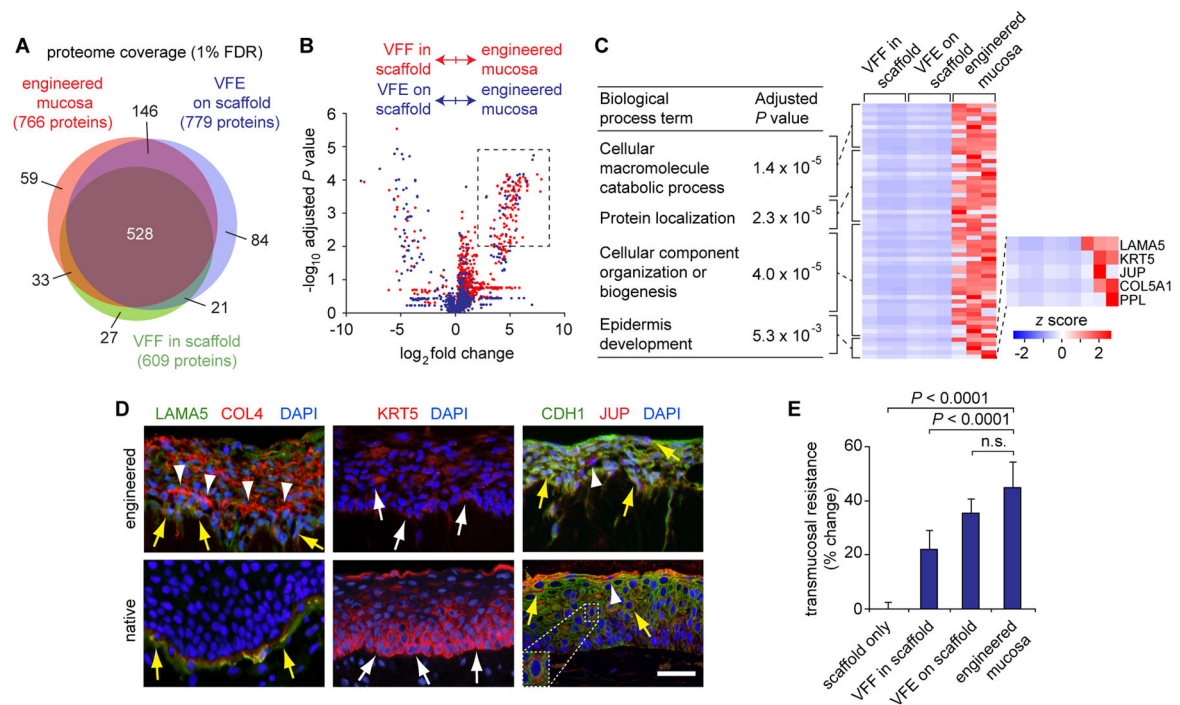


Fig. 3. Proteomic-based analysis of engineered VF mucosa compared to its isolated subcomponents

(A) Venn diagram summarizing proteome coverage across conditions. FDR, false discovery rate. (B) Volcano plot summarizing NSAF-based protein quantification in engineered mucosa versus VFF in scaffold (red) and VFE on scaffold (blue). The dashed rectangle denotes cutoff criteria for protein overrepresentation in engineered mucosa compared to the other conditions. Adjusted *P* values were calculated using a Student's *t* test ($n = 3$). (C) Summary of enriched biological process terms associated with the protein set exclusive to engineered mucosa or overrepresented in engineered mucosa compared to both VFF in scaffold and VFE on scaffold. The table lists the three most highly represented terms (adjusted *P* values were calculated using BiNGO, $n = 3$; postprocessing was performed using REVIGO), as well as the mechanistically relevant epidermis (in the context of mucosa, epithelium) development term. A complete list of enriched terms is presented in table S6. The heatmap shows the relative abundance of overrepresented proteins that map to these terms of interest. (D) Immunohistochemical validation of overrepresented proteins LAMA5 (costained with COL4), KRT5, and JUP (costained with CDH1), in engineered and native VF mucosae. White arrows indicate KRT5⁺ VFE; white arrowheads indicate COL4⁺ signals in the deep epithelium and JUP⁺ VFE; yellow arrows indicate LAMA5⁺COL4⁺ basal VFE in engineered mucosa, LAMA5⁺COL4⁺ basement membrane structures in native mucosa, and CDH1⁺JUP⁺ VFE. Scale bar, 50 μ m; 25 μ m (inset). (E) Transmucosal electrical resistance. Data are means \pm SEM ($n = 4$). *P* values were calculated using ANOVA; n.s., not significant.

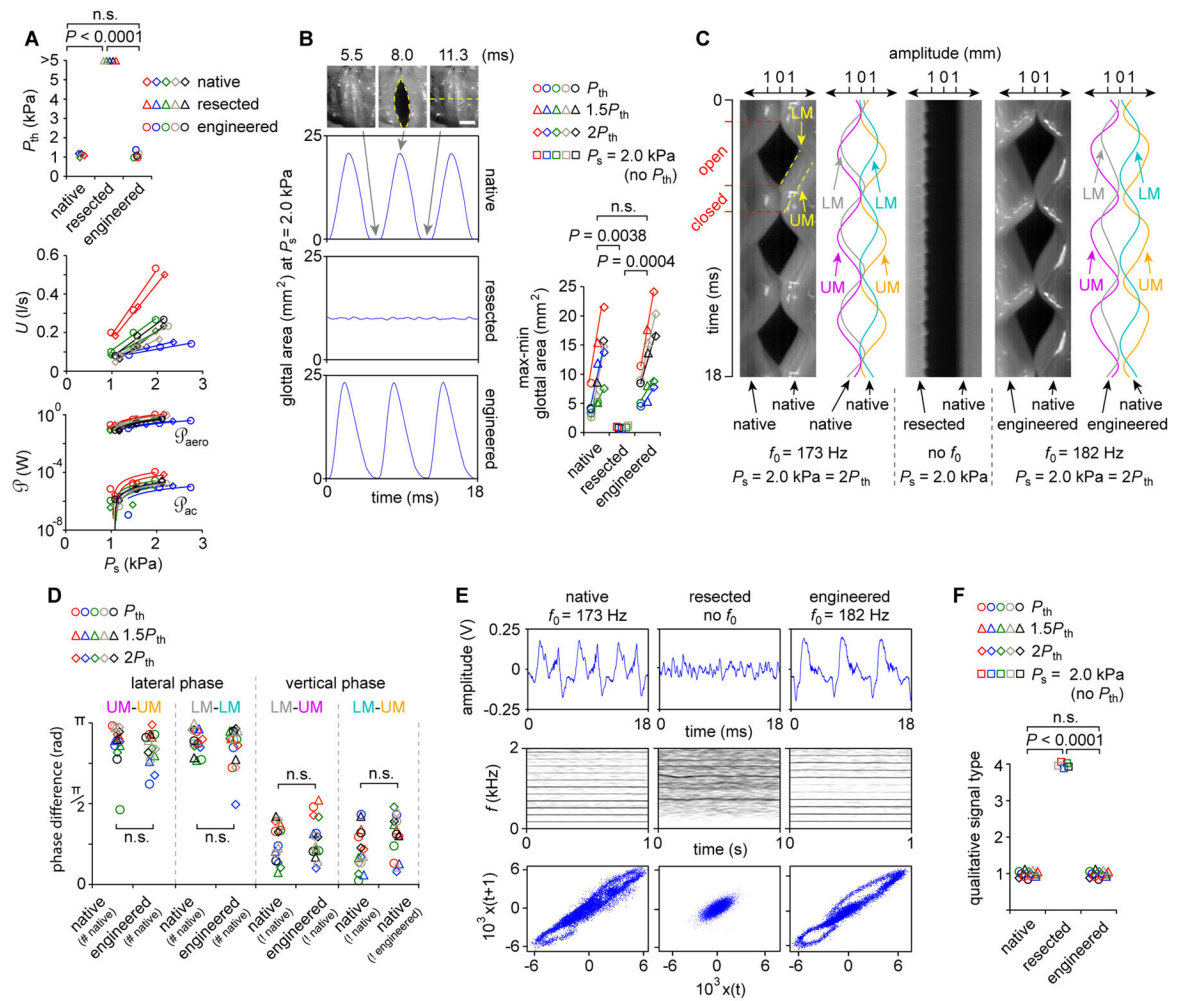


Fig. 4. Ex vivo physiologic performance of engineered VF mucosa in a canine excised larynx (A) Aerodynamic data showing phonation threshold pressure (P_{th}), subglottal pressure (P_s) and flow (U) relationships (i.e., glottal resistance [R_g]); as well as aerodynamic input power (ρ_{aero}) and radiated acoustic output power (ρ_{ac}) relationships (i.e., glottal efficiency [E_g]). P values were calculated using ANOVA. (B) HSDI-based glottal area analysis. Grey arrows indicate the beginning, midpoint and endpoint of a representative 5.8-ms vibratory cycle. The yellow dashed ellipse indicates maximum glottal area. The yellow dashed line indicates the scanning line used for subsequent kymography. Scale bar, 3 mm. P values were calculated using ANOVA. (C) Representative kymograms from the larynx presented in (B). Red tick marks and dashed lines indicate open and closed phases of a single vibratory cycle. Yellow dashed lines indicate the upper and lower VF margins (UM and LM). Sinusoidal curve fitting ($R^2 > 0.98$) to the UM and LM is shown for the native and engineered conditions. f_0 , fundamental frequency. (D) Lateral and vertical phase differences for all larynges and conditions. #, contralateral VF mucosa condition used to calculate lateral phase difference; !, VF mucosa condition contralateral to that for which vertical phase difference is calculated. P values were calculated using ANOVA. (E) Representative acoustic data showing time-domain signals (upper), narrowband spectrograms (center) and phase plots

(lower). **(F)** Qualitative acoustic signal typing for all larynges and conditions. *P* values were calculated using a χ^2 test. Data from a parallel experiment evaluating the *ex vivo* physiologic performance of human oral mucosa are presented in Fig. 5. Data from the same larynx (*n* = 5) are plotted in the same color (A, B, D, F); n.s., not significant.

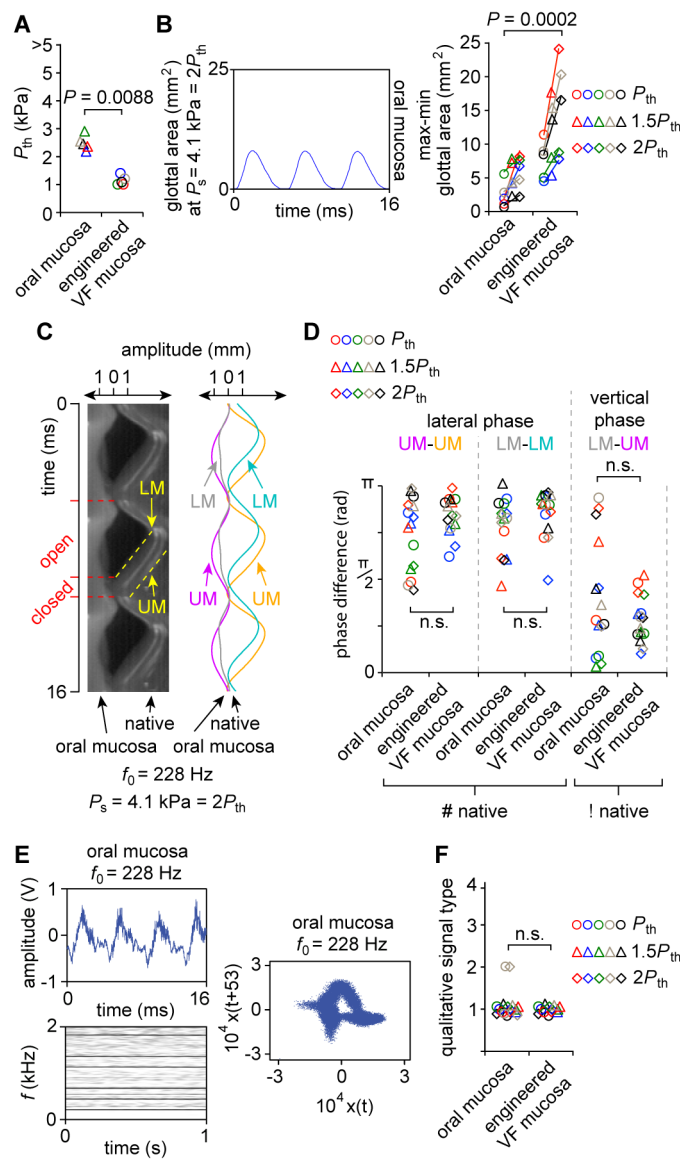


Fig. 5. Ex vivo physiologic performance of human oral mucosa, compared to that of engineered VF mucosa, in a canine excised larynx

(A) Phonation threshold pressure (P_{th}). P values were calculated using a Student's t test. (B) HSDI-based glottal area analysis. P_s , subglottal pressure. P values were calculated using ANOVA. (C) Representative kymogram from the larynx presented in (B). Red tick marks and dashed lines indicate open and closed phases of a single vibratory cycle. Yellow dashed lines indicate the upper and lower VF margins (UM and LM). Sinusoidal curve fitting ($R^2 > 0.98$) to the UM and LM is also shown. f_0 , fundamental frequency. (D) Lateral and vertical phase differences for all larynges and conditions. #, contralateral VF mucosa condition used to calculate lateral phase difference; !, VF mucosa condition contralateral to that for which vertical phase difference is calculated. P values were calculated using ANOVA. (E) Representative acoustic data showing a time-domain signal (upper), narrowband spectrogram (lower) and phase plot (right). (F) Qualitative acoustic signal typing. The P

value was calculated using a χ^2 test. The engineered VF mucosa dataset used for statistical comparisons is presented in complete form in Fig. 4. Data from the same larynx ($n = 5$) are plotted in the same color (A, B, D, F); n.s., not significant.

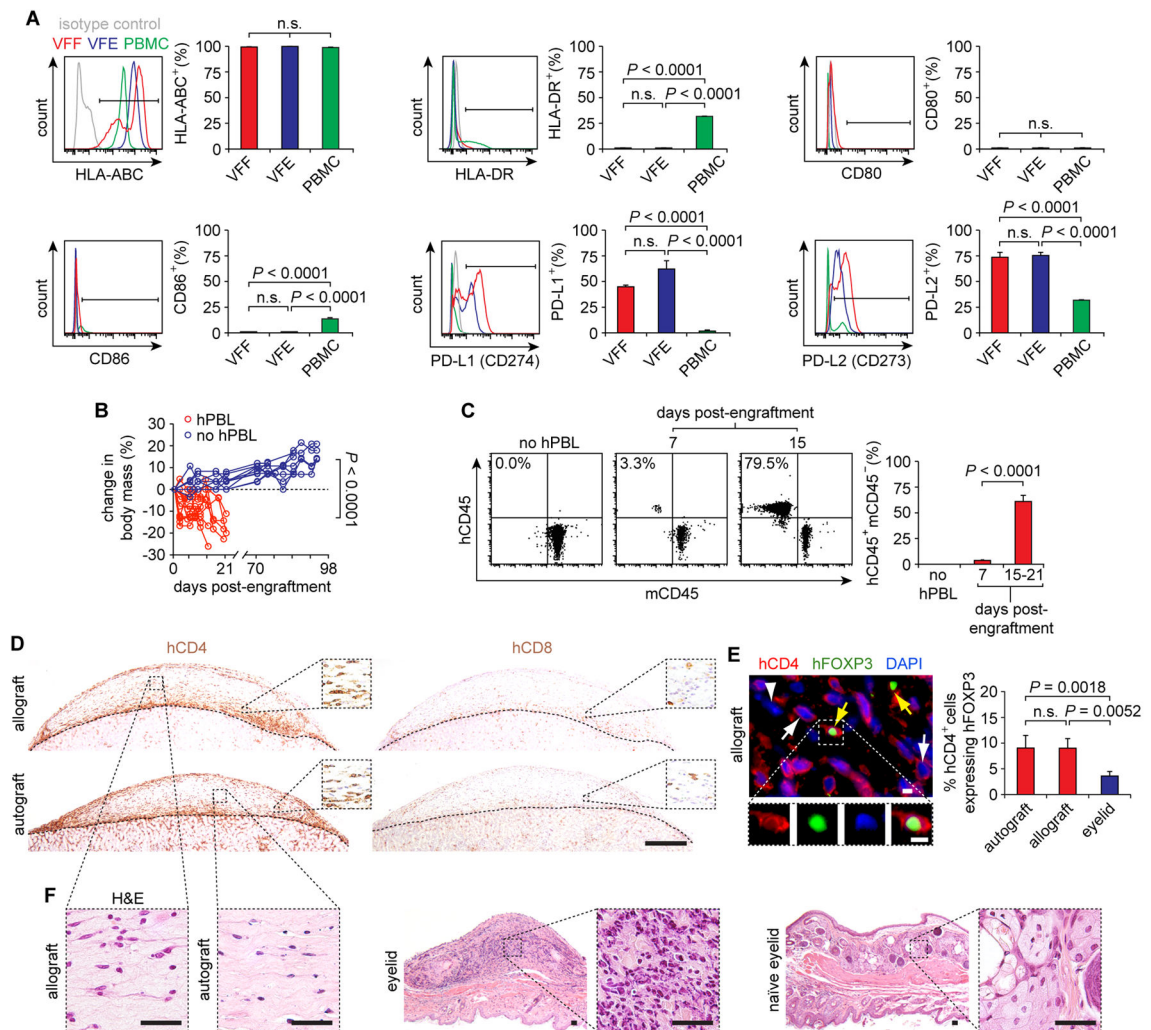


Fig. 6. Immunogenicity of engineered VF mucosa

(A) Expression of cell surface markers HLA-ABC, HLA-DR, CD80, CD86, PD-L1 (CD274) and PD-L2 (CD273) in VFF and VFE compared to peripheral blood mononuclear cell (PBMC) control. Data are means \pm SEM ($n = 5$). P values were calculated using ANOVA. (B) Body mass of NSG mice following hPBL injection, compared to no hPBL control mice ($n = 10-12$). Mice were euthanized following a $>15\%$ decrease in body mass and clinical signs of xenogeneic GVHD, which occurred 15–21 d post-hPBL injection. P values (comparison of total percentage change) were calculated using a Student's t test. (C) hCD45⁺mCD45⁻ human lymphocytes in the peripheral blood of NSG mice following hPBL injection. Data are means \pm SEM ($n = 7-8$). P values were calculated using a Student's t test. (D) hCD4⁺ T helper cell and hCD8⁺ cytotoxic T cell infiltration of the engineered auto- and allografts, 15 d post-hPBL engraftment. Dashed black contour lines indicate the boundaries between the engineered human grafts (top) and the mouse kidneys (bottom). Scale bar, 500 μ m; 70 μ m (insets). (E) hFOXP3 expression by infiltrating hCD4⁺ T cells in the engineered allograft, 15 d post-hPBL engraftment. White arrows indicate hCD4⁺hFOXP3⁻ T helper cells; yellow arrows indicate hCD4⁺hFOXP3⁺ regulatory T cells;

the white arrowhead indicates a hCD4⁺hFOXP3⁺ cell. Scale bars, 5 μ m. The bar graph summarizes cell count data from the engineered auto- and allografts and mouse eyelid, a GVHD positive control tissue. Data are means \pm SEM ($n = 3-6$). *P* values were calculated using ANOVA. (F) H&E-stained sections showing morphology of the engineered auto- and allografts compared to the mouse eyelid, 15 d post-hPBL engraftment. Scale bars, 50 μ m. n.s., not significant.